

Fast Inverse Nonlinear Fourier Transform For Generating Multi-Solitons In Optical Fiber

Sander Wahls

Delft Center for Systems and Control
TU Delft, Delft, The Netherlands
Email: s.wahls@tudelft.nl

H. Vincent Poor

Department of Electrical Engineering
Princeton University, Princeton, NJ, USA
Email: poor@princeton.edu

Abstract—The achievable data rates of current fiber-optic wavelength-division-multiplexing (WDM) systems are limited by nonlinear interactions between different subchannels. Recently, it was thus proposed to replace the conventional Fourier transform in WDM systems with an appropriately defined nonlinear Fourier transform (NFT). The computational complexity of NFTs is a topic of current research. In this paper, a fast inverse NFT algorithm for the important special case of multi-solitonic signals is presented. The algorithm requires only $\mathcal{O}(D \log^2 D)$ floating point operations to compute D samples of a multi-soliton. To the best of our knowledge, this is the first algorithm for this problem with \log^2 -linear complexity. The paper also includes a many samples analysis of the generated nonlinear Fourier spectra.

Index Terms—Nonlinear Fourier Transform, Fast Algorithms, Optical fiber, Nonlinear Schrödinger Equation, Solitons

I. INTRODUCTION

The current generation of fiber-optic communication systems based on wavelength-division-multiplexing (WDM) is operating close to capacity [1]. In order to avoid a looming capacity crunch, new approaches beyond WDM need to be explored. The nonlinear effects in optical fiber lead to interference between different subchannels, and have been identified as one of the major capacity-limiting factors. In order to avoid interference between subchannels, it was recently proposed to modulate information using a nonlinear Fourier transform (NFT) instead of the traditional Fourier transform used in WDM [2], [3], [4]. Analogously to how the spatial evolution of a signal in a linear channel such as copper cable becomes trivial in the traditional Fourier domain, the evolution of a signal in optical fiber becomes trivial in a properly defined nonlinear Fourier domain. The most important aspect here is that different regions in the nonlinear Fourier domain do not interact as the signal travels through the fiber. Thus, by defining subchannels in the nonlinear Fourier domain, interference among them can be avoided. There are many interesting open questions regarding information transmission in the nonlinear Fourier domain, with one of them being computational complexity. While the celebrated fast Fourier transform has been the workhorse of practical implementations of WDM, the first fast NFTs have been proposed only recently [5], [6]. The inverse NFT however, in contrast to the traditional case, differs from the forward transform. No fast inverse NFT

has been established in the literature so far to the best of our knowledge, although inverse NFTs are used in several practical problems [7], [8]. The goal of this paper is to, at least partially, close this gap for the important case of multi-solitonic signals. The algorithm developed in this paper can generate multi-solitons with arbitrary discrete spectra (but not norming constants). Such signals have recently been considered for information transmission in [4] and [9].

The paper is structured as follows. In Section II, the continuous-time NFT is introduced and discretized. The proposed algorithm will operate in two stages, which are then developed in the Sections III and IV. Two numerical examples follow in Section V. Section VI finally concludes the paper.

II. NONLINEAR FOURIER TRANSFORM

In this section, the nonlinear Fourier transform is first established for continuous-time signals. The NFT is then discretized and, finally, the inverse discrete NFT is discussed.

A. Continuous-Time Transform

The nonlinear Fourier transform [w.r.t. the signal model in Eq. (8) below] is due to Zakharov and Shabat [10]. Let $\{q(t)\}_{t \in \mathbb{R}} \subset \mathbb{C}$ denote a vanishing signal. Its NFT is found through the analysis of the associated scattering problem

$$\frac{d}{dt} \phi(t, \lambda) = \begin{bmatrix} -i\lambda & q(t) \\ -\bar{q}(t) & i\lambda \end{bmatrix} \phi(t, \lambda), \quad (1)$$

$$\phi(t, \lambda) = \begin{bmatrix} e^{-i\lambda t} \\ 0 \end{bmatrix} + o(1), \quad t \rightarrow -\infty. \quad (2)$$

With ϕ_1 and ϕ_2 denoting the components of ϕ , define

$$\alpha(\lambda) := \lim_{t \rightarrow \infty} e^{i\lambda t} \phi_1(t, \lambda), \quad \beta(\lambda) := \lim_{t \rightarrow \infty} e^{-i\lambda t} \phi_2(t, \lambda), \quad (3)$$

where $\lambda \in \mathbb{C}$. The functions α and β are usually not well-defined on the whole complex plane. With some assumptions on the signal $q(t)$, however, the following can be said.

Lemma 1 ([11]). *If there exist positive constants C and κ such that $|q(t)| \leq C e^{-2\kappa|t|}$ for all real t , then:*

- 1) $\alpha(\lambda)$ is analytic in the closed upper half-plane $\Im(\lambda) \geq 0$
- 2) $\alpha(\lambda)$ has finitely many roots $\lambda_1, \dots, \lambda_J$ in $\Im(\lambda) \geq 0$
- 3) $\beta(\lambda)$ is analytic around the real line \mathbb{R} and well-defined at the roots $\lambda_1, \dots, \lambda_J$ of $\alpha(\lambda)$ in $\Im(\lambda) > 0$

This lemma implies that the *reflection coefficient*

$$\hat{q}(\omega) := \frac{\beta(\omega)}{\alpha(\omega)}, \quad \omega \in \mathbb{R}, \quad (4)$$

is well-defined except at finitely many poles. The function β/α is also well-defined at the (complex) roots λ_j . The residual of β/α at these points is, assuming that all λ_j are simple roots, given by

$$\tilde{q}_j := \beta(\lambda_j) / \frac{d\alpha}{d\lambda}(\lambda_j).$$

With these definitions in mind, the *nonlinear Fourier transform* (or *scattering data*) of $q(t)$ is defined as [11, Apdx. 5]

$$\{\hat{q}(\omega)\}_{\omega \in \mathbb{R}}, \quad (\lambda_j, \tilde{q}_j)_{j=1}^J. \quad (5)$$

Please note that the nonlinear Fourier spectrum has a physical interpretation [12]. The reflection coefficient reduces to the linear Fourier transform for signals with small amplitudes. It describes the so-called *radiation* components of the signal. The roots λ_k indicate *solitonic components* in the signal, which are further specified through the norming constants \tilde{q}_k . (Solitons are basically “travelling humps” that have no analogue in linear evolution equations.) A *multi-soliton* is a signal that contains several solitonic components. A signal is *reflectionless* if the reflection coefficient is zero everywhere.

The nonlinear Fourier transform has several properties similar to the conventional Fourier transform [2, Sec. IV.D]. In particular, the effects of shifting or dilating the signal on the nonlinear Fourier transform turn out to be simple:

$$q(t - t_0) \leftrightarrow \{e^{-2i\omega t_0} \hat{q}(\omega)\}, (\lambda_j, e^{-2i\lambda_j t_0} \tilde{q}_j), \quad (6)$$

$$q(t/\eta) \leftrightarrow \{\widehat{|\eta|q}(\eta\omega)\}, (\eta\lambda_j, \widehat{|\eta|q}_j). \quad (7)$$

The most important property is however the following. Consider a space-time signal $\{Q(x, t)\}_{x \geq 0, t \in \mathbb{R}} \subset \mathbb{C}$ that is governed by the *focusing nonlinear Schrödinger equation (NSE)*

$$i \frac{\partial Q}{\partial x} = \frac{\partial^2 Q}{\partial t^2} + |Q|^2 Q. \quad (8)$$

Denote the functions $\alpha(z)$ and $\beta(z)$ that correspond to the signal $q(t) = Q(x, t)$ by $\alpha(x, \lambda)$ and $\beta(x, \lambda)$. Then, [2, V]

$$\alpha(x, \lambda) = \alpha(0, \lambda), \quad \beta(x, \lambda) = e^{-4i\lambda^2 x} \beta(0, \lambda).$$

The focusing NSE describes the evolution of a signal in lossless, noise-free optical fiber [2]. The evolution of a signal thus indeed becomes trivial in the nonlinear Fourier domain.

B. Discrete-Time Transform

In order to compute a numerical approximation of the nonlinear Fourier spectrum (5), the signal $q(t)$ is considered only on a (sufficiently large) finite time interval. Since the effects of time-shifting and dilation are simple [see (6)–(7)], we can choose the interval $[-1, 0]$ in order to simplify the following exposition without loss of generality. In this interval, D equidistant scaled samples

$$Q[n] := \epsilon q\left(-1 + n\epsilon - \frac{\epsilon}{2}\right), \quad \epsilon := \frac{1}{D}, \quad n \in \{1, \dots, D\},$$

are taken in order to represent to signal. It will be convenient to transform the spectral parameter λ as follows:

$$z = z(\lambda) := e^{-2i\lambda\epsilon}, \quad \Re(\lambda) \in \left[-\frac{\pi}{2\epsilon}, \frac{\pi}{2\epsilon}\right]. \quad (9)$$

(The real part of λ has been constrained so that the inverse transform $z \mapsto \lambda(z)$ is well-defined.) Under the assumption that $q(t)$ is piecewise constant and that ϵ is infinitesimal, the scattering problem (1)–(2) reduces to [8, Sec. II]

$$\phi[n, z] := \frac{z^{\frac{1}{2}}}{\sqrt{1 + |Q[n]|^2}} \begin{bmatrix} 1 & z^{-1}Q[n] \\ -\tilde{Q}[n] & z^{-1} \end{bmatrix} \phi[n-1, z], \quad (10)$$

$$\phi[0, z] := z^{-\frac{D}{2}} \begin{bmatrix} 1 \\ 0 \end{bmatrix}. \quad (11)$$

Here, the initial condition (11) was obtained by evaluating (2) at $t = -1$. Similarly, after considering (3) at $t = 0$, the functions $\alpha(\lambda)$ and $\beta(\lambda)$ are approximated by

$$a(z) := \phi_1[D, z], \quad b(z) := \phi_1[D, z]. \quad (12)$$

Note that the complex half-strip $\Re(\lambda) \in [-\frac{\pi}{2\epsilon}, \frac{\pi}{2\epsilon}]$, $\Im(\lambda) > 0$ with respect to the original spectral parameter λ corresponds to the exterior of the unit circle $|z| > 1$. The real interval $[-\frac{\pi}{2\epsilon}, \frac{\pi}{2\epsilon}]$, in particular, is mapped to the unit circle $|z| = 1$. The reflection coefficient $\hat{q}(\omega)$ is therefore approximated as

$$\hat{Q}(\omega) := \frac{b(z(\omega))}{a(z(\omega))}, \quad \omega \in \left[-\frac{\pi}{2\epsilon}, \frac{\pi}{2\epsilon}\right]. \quad (13)$$

The roots z_1, \dots, z_K of $a(z)$ outside the unit circle $|z| > 1$ are taken as approximations of the roots $\lambda_1, \dots, \lambda_J$ of $\alpha(\lambda)$ subject to the coordinate transform (9). Note that there may be spurious roots z_k that do not correspond to any of the λ_j . These spurious roots are numerical artifacts. They usually occur in physically unphysical regions (e.g., very close to or very far away from the unit circle) so that they can be easily filtered out. The norming constants \tilde{q}_j are approximated through

$$\tilde{Q}_k := b(z_k) / \frac{da}{dz} \frac{dz}{d\lambda}(\lambda_k) = -\frac{b(z_k)}{2i\epsilon z_k} / \frac{da}{dz}(z_k). \quad (14)$$

The *discrete nonlinear Fourier transform* is then defined by

$$\{\hat{Q}(\omega)\}_{\omega \in [-\frac{\pi}{2\epsilon}, \frac{\pi}{2\epsilon}]}, \quad \{z_k, \tilde{Q}_k\}_{k=1}^K. \quad (15)$$

C. Inverse Discrete-Time Transform

A close look at the finite difference equation (10) reveals that $a(z)$ and $b(z)$ defined in (12) are necessarily polynomials of z^{-1} with a degree of at most D [8, (19)]:

$$a(z) = \sum_{i=0}^{D-1} a_i z^{-i}, \quad b(z) = \sum_{i=0}^{D-1} b_i z^{-i}. \quad (16)$$

Please note that the additional factors $z^{D/2}$ given in [8, (19)] cancel with the factor in (11) in our case. The following lemma specifies the range of the discrete nonlinear Fourier transform.

Lemma 2 ([8]). *Fix two arbitrary polynomials as in (16). Then, there exists samples $Q[1], \dots, Q[D]$ such that (12) is satisfied*

if and only $a_0 \geq 0$ and $|a(\xi)|^2 + |b(\xi)|^2 = 1$ for all $|\xi| = 1$. In that case, $a_0 = 1/\prod_{n=1}^D \sqrt{1 + |Q[n]|^2} > 0$ and

$$Q[D] = \frac{a_{D-1}}{b_{D-1}} = -\frac{\bar{b}_0}{\bar{a}_0}. \quad (17)$$

Proof: The first part is shown in [8, Sec. IV+Apdx.]. The other two formulas are given in [8, Eqs. (14a)+(15)+(37)]. The last formula deviates from [8] because here $Q[n] = -\bar{\rho}_n$. ■

There are various ways to approach the inverse nonlinear Fourier transform. See, e.g., [4]. The fast $\mathcal{O}(D \log^2 D)$ algorithm that will be proposed in the following two sections uses a two-step procedure similar to [8] and [12]:

- 1) Synthesize $a(z)$ and $b(z)$ such that the conditions in Lemma 2 are met and the roots of $a(z)$ are $z_k := z(\lambda_k)$.
- 2) Recover the samples $Q[n]$ from (10)–(11).

The complexities of comparable algorithms are higher: either $\mathcal{O}(D^2)$, as in [12] and [8]; $\mathcal{O}(DK^2)$ as in [7] and [4, III.B-3]; or even $\mathcal{O}(D^3)$ as in [4, III.B-1]. Here K is the number of solitons. (Note that $K \sim D$ in communication problems.)

III. STEP 1: FAST GENERATION OF $a(z)$ AND $b(z)$

In this section, the first step of our proposed algorithm is described. The basic approach used here is due to our previous work [12]. However, the construction given here avoids a pathology from which the construction in [12] suffers, as a new many-samples analysis presented below shows. Please note that no complexity analysis of this step will be given here because the analysis given in [12, VI] still applies.

A. Basic Construction

Consider any polynomial $\psi(z) = \sum_{i=0}^{D-1} \psi_i z^{-i}$ that fulfills

$$|\psi(z)| \in [0, 1] \quad \forall |z| = 1.$$

Through spectral factorization [13], two polynomials $u(z) = \sum_{i=0}^{D-1} u_i z^{-i}$ and $b(z) = \sum_{i=0}^{D-1} b_i z^{-i}$ can be found that have no roots outside the unit circle and satisfy

$$|u(\xi)|^2 = 1 - \delta^2 |\psi(\xi)|^2, \quad |b(\xi)|^2 = \delta^2 |\psi(\xi)|^2 \quad \forall |\xi| = 1. \quad (18)$$

Here, $\delta \in (0, 1)$ is a free parameter. We choose

$$a_{\text{ideal}}(z) := u(z) \prod_{k=1}^K \frac{z - z_k}{1 - z\bar{z}_k}. \quad (19)$$

This ideal $a_{\text{ideal}}(z)$ has the right roots in $|z| > 1$ and satisfies

$$|a_{\text{ideal}}(\xi)|^2 + |b(\xi)|^2 = |u(\xi)|^2 \prod_{k=1}^K |\xi| \frac{|\xi - z_k|}{|\xi - \bar{z}_k|} + |b(\xi)|^2$$

(use $|\xi| = 1$) $= 1 - \delta^2 |\psi(\xi)|^2 + \delta^2 |\psi(\xi)|^2 = 1, \quad (20)$

for all $|\xi| = 1$, but it is not a polynomial in z^{-1} , in general.

However, since $a_{\text{ideal}}(z)$ is rational with all poles inside the unit circle, it has an expansion $a_{\text{ideal}}(z) = \sum_{i=0}^{\infty} a_{\text{ideal},i} z^{-i}$ in $|z| \geq 1$ with coefficients that vanish exponentially fast. Thus, $a_{\text{ideal}}(z)$ can be easily approximated by a polynomial $p(z) = \sum_{i=0}^{D-1} p_i z^{-i}$ up to any desired precision given that D

is not too small. We shall assume this in the following, and set

$$a(z) := e^{i\varphi} \sum_{i=0}^{D-1} p_i z^{-i} = e^{i\varphi} a_{\text{ideal}}(z) + \mathcal{O}(\epsilon^2),$$

where $\varphi \in [-\pi, \pi]$ is such that $a(z)$ fulfills the condition $\lim_{z \rightarrow \infty} a(z) \geq 0$ in Lemma 2. In light of (20), one finds that $a(z)$ and $b(z)$ also fulfill the other condition in Lemma 2 (up to a rapidly vanishing error). Thus, the problem of recovering $Q[1], \dots, Q[D]$ through (10)–(11) is well-defined.

B. Choice Of The Filter $\psi(z)$

In our previous paper [12], the filter $\psi(z) = z^{-(D-1)}$ and a very small δ were used. However, an analysis similar to the one below shows that this choice results in a reflection coefficient that does not vanish in the many samples regime for $\omega \rightarrow \pm\infty$. Parseval's identity for the NFT [2, p. 4320] however implies that any reflection coefficient of a signal with finite energy must vanish. Although this can be fixed by letting δ depend on ϵ , one then obtains the problem that the norming constants converge towards zero as $D \rightarrow \infty$. Again, this cannot happen for any real signal. In order to avoid these two problems, one may fix δ independently of ϵ and use a proper low-pass filter for $\psi(z)$ to ensure that the reflection coefficient vanishes at higher frequencies. In our numerical experiments, a simple truncated ideal low-pass was used [14, p. 98]:

$$\psi(z) := \sum_{i=0}^{D-1} \frac{2\omega_c}{D\pi} \text{sinc}\left(\frac{2\omega_c}{D\pi} \left(i - \frac{D-1}{2}\right)\right) z^{-i}, \quad (21)$$

where $\omega_c = 10$ is the desired cut-off frequency for the reflection coefficient (4). Please note that the filter $\psi(z)$ is independent of $q(t)$ and thus needs to be designed only once.

C. Many Samples Analysis

In this subsection, the continuous-time nonlinear Fourier spectrum (5) that is generated through $a(z)$ and $b(z)$ introduced above is analyzed in the many samples regime $D = 1/\epsilon \rightarrow \infty$. The function $a(z)$ is constructed such that its roots in $|z| > 1$ match exactly the prespecified $\lambda_1, \dots, \lambda_K$ under the transform $\lambda \mapsto z(\lambda)$. The behavior of the reflection coefficient can be analyzed using (13), (18) and (20):

$$|\hat{q}(\omega)|^2 = \lim_{D \rightarrow \infty} |\hat{Q}(\omega)|^2 = \frac{\delta^2 |\Psi(\omega)|^2}{1 - \delta^2 |\Psi(\omega)|^2}, \quad \omega \in \mathbb{R}. \quad (22)$$

Here, $|\Psi|$ denotes the asymptotic amplitude of (21) given by

$$|\Psi(\omega)| := \lim_{D \rightarrow \infty} |\psi(z(\omega))| = \frac{|\text{Si}(\omega + \omega_c) - \text{Si}(\omega - \omega_c)|}{\pi},$$

where $\text{Si}(s) := \int_0^s \frac{\sin \theta}{\theta} d\theta$ is the *sine integral function* [14, p. 98]. It now follows from $|\Psi(\omega)| \rightarrow \pm \frac{\pi}{2}$ that $q(\omega) \rightarrow 0$ for $\omega \rightarrow \pm\infty$. That is, the pathology of the construction in [12] discussed in the previous subsection has been fixed with the new design. The norming constants (14) are more difficult to analyze. In the appendix, they are shown to satisfy

$$\tilde{q}_k = \lim_{\epsilon \rightarrow 0} \tilde{Q}_k = -\frac{B(\lambda_k)}{U(\lambda_k)} (\lambda_k - \bar{\lambda}_k) \prod_{i \neq k} -\frac{\lambda_k - \lambda_i}{\lambda_k - \bar{\lambda}_i}, \quad (23)$$

where $B(\lambda) := \lim_{\epsilon \rightarrow 0} b(z(\lambda))$ and $U(\lambda) := \lim_{\epsilon \rightarrow 0} u(z(\lambda))$. This formula shows that the norming constants have finite non-zero limits in the many samples regime unless one of the prespecified λ_k coincides with a root of either $B(\lambda_k)$ and $U(\lambda_k)$. We have not yet performed an exact analysis of $B(\lambda)$ and $U(\lambda)$. But since the functions $B(\lambda)$ and $U(\lambda)$ (and therefore their roots) are independent of the $\lambda_1, \dots, \lambda_K$, it seems unlikely that the pathology of vanishing norming constants discussed above occurs with the new construction.

IV. STEP 2: FAST INVERSE SCATTERING

In this section, $a(z)$ and $b(z)$ are now considered known and the samples $Q[1], \dots, Q[D]$ have to be recovered. A fast inverse scattering algorithm that recovers $Q[1], \dots, Q[D]$ using only $\mathcal{O}(D \log^2 D)$ floating point operations (*flops*) for systems of the form (10) has been proposed by McClary [15, (2)]. Unfortunately, his algorithm does not work in our setup. In [15], the functions $a(z)$ and $b(z)$ are interpreted as z -transforms of a down-going wave, which is sent into the earth, and a resulting upcoming wave, which is measured at the same location. The initial condition (11) corresponds to the situation where a unit pulse is sent into the earth and no upcoming wave is generated, leading to a trivial medium that does not reflect (i.e., $Q[1] = \dots = Q[D] = 0$).

In the following, we will describe how McClary's approach can be modified such that it works in our setup. By inverting (10) and taking the definition (12) of $a(z)$ and $b(z)$ into account, one arrives at the following scattering problem:

$$\begin{aligned} \begin{bmatrix} a_{n-1}(z) \\ b_{n-1}(z) \end{bmatrix} &= \frac{z^{-\frac{1}{2}}}{\theta[n]} \begin{bmatrix} 1 & -Q[n] \\ z\bar{Q}[n] & z \end{bmatrix} \begin{bmatrix} a_n(z) \\ b_n(z) \end{bmatrix} \\ \begin{bmatrix} a_D(z) \\ b_D(z) \end{bmatrix} &= \begin{bmatrix} a(z) \\ b(z) \end{bmatrix}, \quad \theta[n] := \sqrt{1 + |Q[n]|^2}. \end{aligned} \quad (24)$$

Assume that D is even and split

$$a(z) = a^L(z) + z^{-\frac{D}{2}} a^U(z), \quad a^L(z) := \sum_{i=0}^{\frac{D}{2}-1} a_i z^{-i}.$$

Split $b(z) = b^L(z) + z^{-\frac{D}{2}} b^U(z)$ in the same way, and define

$$\mathbf{T}_n(z) := \frac{z^{-\frac{1}{2}}}{\sqrt{1 + |Q[n]|^2}} \begin{bmatrix} 1 & -Q[n] \\ z\bar{Q}[n] & z \end{bmatrix}, \quad (25)$$

$$\mathbf{T}_{m \rightarrow n}(z) := \mathbf{T}_{n+1}(z) \mathbf{T}_{n+2}(z) \times \dots \times \mathbf{T}_m(z).$$

With this notation, one has that

$$\begin{bmatrix} a_{D-m} \\ b_{D-m} \end{bmatrix} = \mathbf{T}_{D \rightarrow m} \begin{bmatrix} a^L \\ b^L \end{bmatrix} + z^{-\frac{D}{2}} \mathbf{T}_{D \rightarrow m} \begin{bmatrix} a^U \\ b^U \end{bmatrix}. \quad (26)$$

This equation leads to the important conclusion that the highest coefficient of a_{D-m} and b_{D-m} is independent of a^U and b^U as long as $m < \frac{D}{2}$ (because $z^{-\frac{D}{2}} \mathbf{T}_{D \rightarrow m}$ will always shift the coefficients of a^U and b^U up in that case.) Since $Q[D-m]$ can be recovered from the highest coefficients through (17), this shows that the iteration (24) with initial condition

$$a_{\frac{D}{2}}(z) = a^U(z), \quad b_{\frac{D}{2}}(z) = b^U(z)$$

can be used to recover $Q[D], \dots, Q[\frac{D}{2} + 1]$. This insight ensures that the divide-and-conquer strategy given in Algorithm 1 indeed recovers $Q[1], \dots, Q[D]$. The computational

Algorithm 1 Recursive inverse scattering (requires $D = 2^d$)

Input: $a(z) = \sum_{i=0}^{D-1} a_i z^{-i}$ and $b(z) = \sum_{i=0}^{D-1} a_i z^{-i}$

Output: $Q[1], \dots, Q[D]$ and $\mathbf{T}_{D \rightarrow 1}(z)$

if $D = 1$:

- **return** $Q[1] = a_0/b_0$ and $\mathbf{T}_1(z)$ in (25)

else:

- call self with inputs $a^U(z)$ and $b^U(z)$ to recover $Q[D], \dots, Q[\frac{D}{2} + 1]$ and $\mathbf{T}_{D \rightarrow D/2}(z)$
 - recover $a_{D/2}(z)$ and $b_{D/2}(z)$ via (26)
 - call self with inputs $a_{D/2}(z)$ and $b_{D/2}(z)$ to recover $Q[D/2], \dots, Q[1]$ and $\mathbf{T}_{D/2 \rightarrow 1}$
 - **return** $Q[1], \dots, Q[D]$ and $\mathbf{T}_{D \rightarrow D/2} \mathbf{T}_{D/2 \rightarrow 1}$
-

bottleneck in Algorithm 1 are the polynomial products. By applying the same complexity analysis that was used for [6, Alg. 1] to the recursion tree generated by Algorithm 1, one finds that its overall complexity is $\mathcal{O}(D \log^2 D)$ flops if the fast Fourier transform is used to multiply polynomials efficiently.

V. NUMERICAL EXAMPLES

In the first example, a single soliton with a root at $\lambda_1 = 20i$ is considered. For small $\delta > 0$, the generated signal will be almost reflectionless. For several number of samples D and δ 's, the two steps of our algorithm as described in Sections III and IV have been carried out. Then, the forward NFT was used to compute the norming constants of the generated signal. Reflectionless signals with one soliton have a well-known closed-form solution (e.g., [12, II.D]). We used this analytical solution to generate samples $Q_{\text{exact}}[n]$ that represent the exact one-soliton with the prespecified λ_1 and the numerically determined norming constant. The error between the generated signal and the analytical solution is depicted in Figure 1 (left). It eventually saturates because the generated signal is not exactly reflectionless, but the error floors decrease as δ is decreased. The normalized runtimes are presented in Figure 1 (right). The runtime per sample grow only very slowly with D , confirming the overall $\mathcal{O}(D \log^2 D)$ runtime. (The runtimes do not include the generation of $u(z)$ and $B(z)$ because they are independent of the signal and have to be computed only once.)

The second example considers a problem from [9]. A multi-soliton with roots at $\lambda_k = 0.25ik$, $k \in \{1, \dots, 4\}$, is generated. The roots were scaled by a factor $\eta = 50$ such that the signal would fit in the interval $[-1, 0]$ (see (7)). The generated signal was rescaled to the original time-scale and analyzed using the forward NFT. The results are depicted in Figure 2. The forward NFT found the roots λ_k of the generated signal exactly in the right places. The reflection coefficient looks as predicted in (22). It is interesting to compare Figure 2 (left) with [9, Fig. 2b]. It was expected that the signals are different due to different norming constants. However, our signal has approximately the same duration, but with only half as many extrema. The highest peak is also about only half as high as in [9, Fig. 2b]. We speculate that the roots in [9,

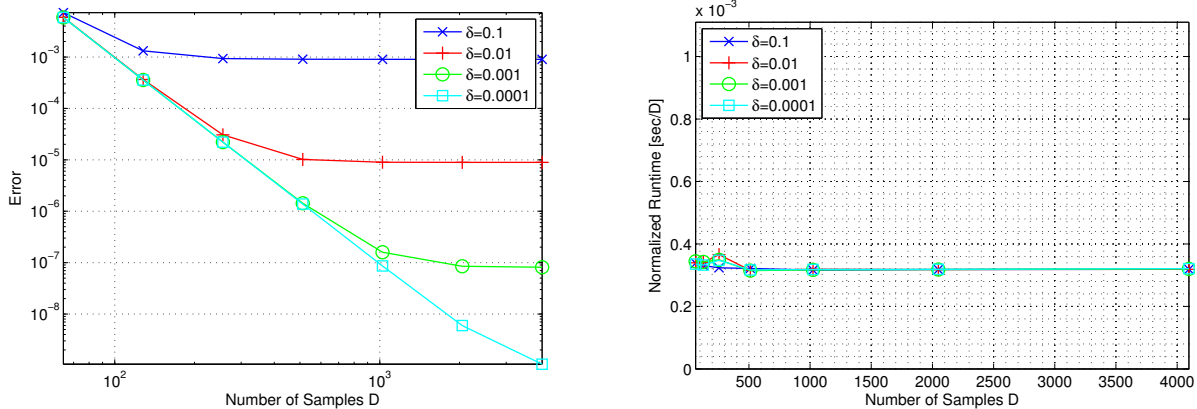


Figure 1. First example. Left: Squared error $\sum_{n=1}^D |Q[n] - Q_{\text{exact}}[n]|^2 / \sum |Q_{\text{exact}}[n]|^2$. Right: Runtime per sample.

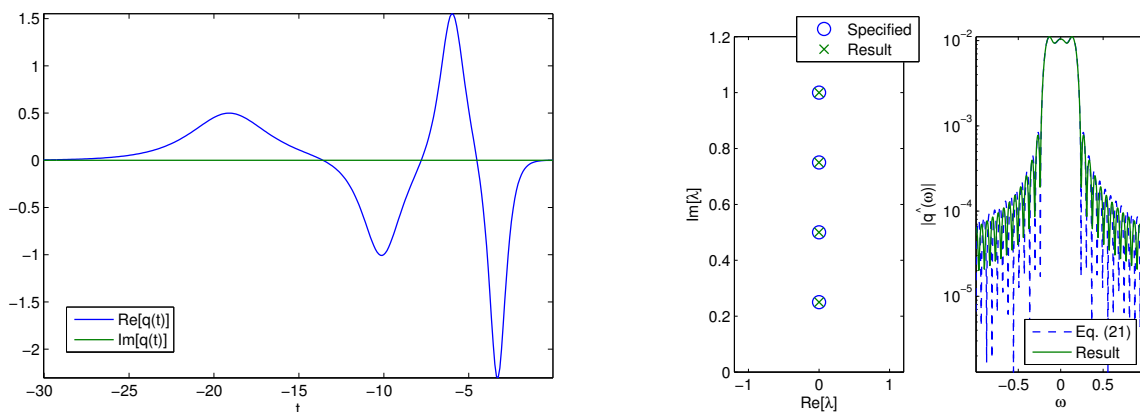


Figure 2. Second example. Left: Generated time-domain signal ($D = 512$, $\delta = 0.01$). Right: Roots of $a(z(\lambda))$ and reflection coefficient.

Fig. 2b) may be double because these quantitative differences vanish if the orders of the roots are doubled in our algorithm.

VI. CONCLUSIONS

The (to the best of our knowledge) first fast inverse nonlinear Fourier transform for the generation of multi-solitons has been presented. The generated nonlinear Fourier spectra have been analyzed through a many samples analysis. The $\mathcal{O}(D \log^2 D)$ runtime and accuracy of the algorithm have also been confirmed experimentally. The current algorithm offers only rough control over the reflection coefficient and norming constants, which should be addressed in future research.

REFERENCES

- [1] R. Essiambre, G. Kramer, P. J. Winzer, G. J. Foschini, and B. Goebel, "Capacity limits of optical fiber networks," *J. Lightwave Technol.*, vol. 28, no. 4, pp. 662–701, Feb. 2010.
- [2] M. I. Yousefi and F. R. Kschischang, "Information transmission using the nonlinear Fourier transform, Part I: Mathematical tools," *IEEE Trans. Inf. Theory*, vol. 60, no. 7, pp. 4312–4328, Jul. 2014.
- [3] —, "Information transmission using the nonlinear Fourier transform, Part II: Numerical methods," *IEEE Trans. Inf. Theory*, vol. 60, no. 7, pp. 4329–4345, Jul. 2014.
- [4] —, "Information transmission using the nonlinear Fourier transform, Part III: Spectrum modulation," *IEEE Trans. Inf. Theory*, vol. 60, no. 7, pp. 4346–4369, Jul. 2014.
- [5] S. Wahls and H. V. Poor, "Introducing the fast nonlinear Fourier transform," in *Proc. IEEE Int. Conf. Acoust. Speech Signal Process. (ICASSP)*, Vancouver, Canada, May 2013.
- [6] —, "Fast numerical nonlinear Fourier transforms," Preprint submitted to *IEEE Trans. Inf. Theory*, Oct. 2014, arXiv:1402.1605v2 [cs.IT].
- [7] D. E. Rourke and P. G. Morris, "Half solitons as solutions to the Zakharov-Shabat eigenvalue problem for rational reflection coefficient with application in the design of selective pulses in nuclear magnetic resonance," *Phys. Rev. A*, vol. 46, no. 7, pp. 3631–3636, 1992.
- [8] J. K. Brenne and J. Skaar, "Design of grating-assisted codirectional couplers with discrete inverse-scattering algorithms," *J. Lightwave Technol.*, vol. 21, no. 1, pp. 254–263, Jan. 2003.
- [9] S. Hari, F. Kschischang, and M. Yousefi, "Multi-eigenvalue communication via the nonlinear Fourier transform," in *Proc. Bien. Symp. Commun.*, Kingston, ON, Canada, Jun. 2014, pp. 92–95.
- [10] V. F. Zakharov and A. B. Shabat, "Exact theory of two-dimensional self-focusing and one-dimensional self-modulation of wave in nonlinear media," *Sov. Phys. JETP*, vol. 34, no. 1, pp. 62–69, Jan. 1972.
- [11] M. J. Ablowitz, D. J. Kaup, A. C. Newell, and H. Segur, "The inverse scattering transform – Fourier analysis for nonlinear problems," *Stud. Appl. Math.*, vol. 53, pp. 249–315, 1974.
- [12] S. Wahls and H. V. Poor, "Inverse nonlinear Fourier transforms via interpolation: The Ablowitz-Ladik case," in *Proc. Int. Symp. Math. Theory Networks Systems (MTNS)*, Groningen, The Netherlands, Jul. 2014, pp. 1848–1855.
- [13] A. H. Sayed and T. Kailath, "A survey of spectral factorization methods," *Numer. Linear Algebra Appl.*, vol. 8, pp. 467–496, 2001.
- [14] A. Papoulis, *The Fourier Integral And Its Applications*. McGraw-Hill, 1962.
- [15] W. K. McClary, "Fast seismic inversion," *Geophysics*, vol. 48, no. 10, pp. 1371–1372, Oct. 1983.

APPENDIX: DERIVATION OF EQUATION (23)

The transformed coordinate $z = e^{-2i\lambda\epsilon}$ will be close to one in the many samples regime $\epsilon = 1/D \rightarrow 0$. The usual first order approximation of the exponential around zero,

$$e^s = \sum_{i=0}^{\infty} \frac{s^i}{i!} = 1 + s + \mathcal{O}(|s|^2),$$

shows that

$$z = 1 - 2i\lambda\epsilon + \mathcal{O}(\epsilon^2)$$

and

$$\bar{z} = e^{2i\bar{\lambda}\epsilon} = 1 + 2i\bar{\lambda}\epsilon + \mathcal{O}(\epsilon^2).$$

From these two formulas, one finds that

$$\begin{aligned} \frac{z - z_i}{1 - z\bar{z}_i} &= \frac{(1 - 2i\lambda\epsilon + \mathcal{O}(\epsilon^2)) - (1 - 2i\lambda_i\epsilon + \mathcal{O}(\epsilon^2))}{1 - (1 - 2i\lambda\epsilon + \mathcal{O}(\epsilon^2))(1 + 2i\bar{\lambda}_i\epsilon + \mathcal{O}(\epsilon^2))} \\ &= -\frac{\lambda - \lambda_i + \mathcal{O}(\epsilon^2)}{\lambda - \bar{\lambda}_i + \mathcal{O}(\epsilon^2)} \end{aligned}$$

and

$$\begin{aligned} \frac{1}{1 - z_k\bar{z}_k} &= \frac{1}{1 - (1 - 2i\lambda_k\epsilon + \mathcal{O}(\epsilon^2))(1 + 2i\bar{\lambda}_k\epsilon + \mathcal{O}(\epsilon^2))} \\ &= \frac{1}{2i\epsilon} \frac{1}{\lambda_k - \bar{\lambda}_k + \mathcal{O}(\epsilon^2)}. \end{aligned}$$

The derivative of the Blaschke product

$$\mathcal{B}(z) := \prod_{i=1}^K \frac{z - z_i}{1 - z\bar{z}_i}$$

that occurs in the definition (19) of $a_{\text{ideal}}(z)$ is given by

$$\frac{d\mathcal{B}}{dz}(z) = \sum_{k=1}^K \frac{1 - |z_k|^2}{(1 - z\bar{z}_k)^2} \prod_{i \neq k} \frac{z - z_i}{1 - z\bar{z}_i},$$

and satisfies

$$\frac{d\mathcal{B}}{dz}(z_k) = \frac{1}{1 - |z_k|^2} \prod_{i \neq k} \frac{z_k - z_i}{1 - z_k\bar{z}_i}.$$

The approximations given above therefore imply that

$$\frac{d\mathcal{B}}{dz}(z_k) = \frac{1}{2i\epsilon} \frac{1}{\lambda_k - \bar{\lambda}_k + \mathcal{O}(\epsilon^2)} \prod_{i \neq k} -\frac{\lambda_k - \lambda_i + \mathcal{O}(\epsilon^2)}{\lambda_k - \bar{\lambda}_i + \mathcal{O}(\epsilon^2)},$$

and thus

$$\begin{aligned} \frac{da}{dz}(z_k) &= \frac{da_{\text{ideal}}}{dz}(z_k) + \mathcal{O}(\epsilon^2) \\ &= \frac{du}{dz}(z_k) \underbrace{\mathcal{B}(z_k)}_{=0} + u(z_k) \frac{d\mathcal{B}}{dz}(z_k) + \mathcal{O}(\epsilon^2) \\ &= \frac{u(z_k)}{2i\epsilon} \frac{1}{\lambda_k - \bar{\lambda}_k + \mathcal{O}(\epsilon^2)} \prod_{i \neq k} -\frac{\lambda_k - \lambda_i + \mathcal{O}(\epsilon^2)}{\lambda_k - \bar{\lambda}_i + \mathcal{O}(\epsilon^2)} \\ &\quad + \mathcal{O}(\epsilon^2). \end{aligned}$$

Equation (23) now follows when the previous formula is plugged into (14):

$$\tilde{Q}_k = -\frac{b(z_k)}{2i\epsilon z_k} \bigg/ \left(\frac{u(z_k)}{2i\epsilon} \frac{1}{\lambda_k - \bar{\lambda}_k + \mathcal{O}(\epsilon^2)} \right),$$

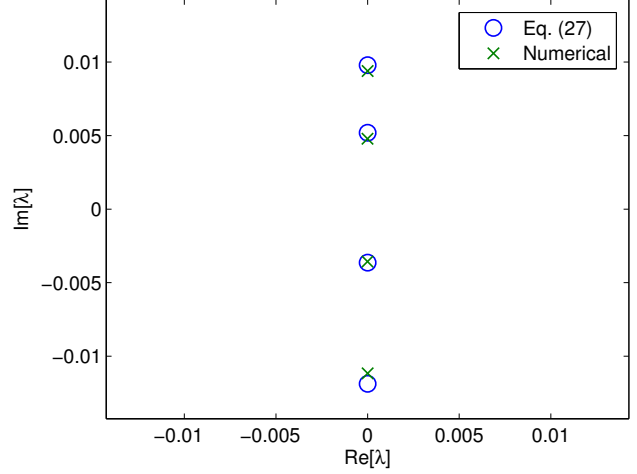


Figure 3. Norming constants for the second numerical experiment

$$\begin{aligned} &\times \prod_{i \neq k} -\frac{\lambda_k - \lambda_i + \mathcal{O}(\epsilon^2)}{\lambda_k - \bar{\lambda}_i + \mathcal{O}(\epsilon^2)} + \mathcal{O}(\epsilon^2) \\ &= -\frac{b(z_k)}{z_k} \bigg/ \left(\frac{u(z_k)}{1} \frac{1}{\lambda_k - \bar{\lambda}_k + \mathcal{O}(\epsilon^2)} \right) \\ &\times \prod_{i \neq k} -\frac{\lambda_k - \lambda_i + \mathcal{O}(\epsilon^2)}{\lambda_k - \bar{\lambda}_i + \mathcal{O}(\epsilon^2)} + \mathcal{O}(\epsilon^2) \\ &\xrightarrow{\epsilon \rightarrow 0} -\frac{B(\lambda_k)}{U(\lambda_k)} (\lambda_k - \bar{\lambda}_k) \prod_{i \neq k} -\frac{\lambda_k - \bar{\lambda}_i}{\lambda_k - \lambda_i}, \end{aligned}$$

where $U(\lambda)$ and $B(\lambda)$ have been defined in Section III-C.

We have not yet analyzed the limits $U(\lambda)$ and $B(\lambda)$, as was already mentioned in Section III-C. However, we compared the prediction made by the semi-asymptotic formula

$$\tilde{Q}_k \approx -\frac{b(z_k)}{u(z_k)} (\lambda_k - \bar{\lambda}_k) \prod_{i \neq k} -\frac{\lambda_k - \bar{\lambda}_i}{\lambda_k - \lambda_i}. \quad (27)$$

with the exact norming constants that were determined numerically for the second numerical experiment in order to investigate how fast the norming constants converge towards their many samples limit. The results are shown in Figure 3. The values obtained from (27) match the true norming constants quite well, but not as well as the roots match their desired values in Figure 2 (right). This is consistent with the results reported in [3, p. 4339], where it was found that the norming constants (or *spectral amplitudes*) converge slowly.